

A comparison of viscoelastic stress wakes for 2D and 3D Newtonian drop deformation in a viscoelastic matrix under shear

S. Afkhami,* P. Yue,[†] and Y. Renardy[‡]

Department of Mathematics, 460 McBryde Hall, Virginia Tech, Blacksburg VA 24061-0123, USA

(Dated: June 23, 2009)

A recent experimental study of a Newtonian drop suspended in a viscoelastic matrix undergoing simple shear displays a transient overshoot in drop deformation which is qualitatively similar to 2D numerical simulation results. Despite the similarity, an interpretation in light of the 2D result is misleading because the overshoot is absent in the fully 3D simulation. This motivates a study of regimes where qualitatively different and interesting features such as overshoots in deformation occur for a 2D drop but not for a 3D drop. The influence of viscoelastic ‘wakes’ that emanate from the drop tips is reported. The viscoelastic wakes are larger and of higher magnitude in 3D than in 2D, and lead to more deformation in 3D. During drop evolution, the less deformed drop is found to be aligned more with the flow direction. As the drop to matrix viscosity ratio increases from 1 to past 3, drop rotation is promoted, with accompanying retraction when the capillary number is sufficiently high. Thus, a 3D overshoot in deformation is promoted with increasing viscosity ratio.

PACS numbers: 47.11.-j,47.55D-,47.55.df

I. INTRODUCTION

Recent experimental studies of Newtonian drops suspended in Boger fluids and sheared have been compared with model equations and small deformation asymptotics [1–8]. Higher deformations require a fully numerical approach [9–11] which is computationally expensive because of the need to capture viscoelastic stresses that have large gradients localized next to the drop surface. At this time, a 2D numerical simulation is completed on a PC in a few hours. This would be a reasonable first step, rather than the 3D simulation which uses at least 16 cpus parallelized over a week. Figure 1 compares experimental data for a Newtonian drop in a Boger fluid at drop to matrix viscosity ratio $\lambda = 1.5$, capillary number $Ca = 0.36$, and matrix Weissenberg number $We = 2.12$ [7]. The experimental data are predicted fairly well by the 3D numerical simulation (3D —, 2D - -). The 2D simulation is qualitatively similar but underpredicts the data. On the other hand, there are experimental results that show qualitatively similar behavior as in 2D simulations, but which are qualitatively different from 3D simulations. An example is Fig. 11 in [8], where the experimental data undergo transient overshoots before settling down to steady state shapes. Coincidentally, this behavior is qualitatively similar to 2D simulations, but not the 3D simulations. We note that the lack of an overshoot in our 3D simulation is corroborated by [11]. This raises a question about the interpretation of experimental data in the light of the less computationally expen-

sive 2D option. We shall investigate a case where the 2D or initially cylindrical drop undergoes an elongation followed by retraction while the 3D or initially spherical drop grows gradually in deformation toward a steady state or to breakup for large values of Ca .

We consider a Newtonian drop of initial radius R_0 and viscosity η_d , suspended in a viscoelastic matrix of total viscosity $\eta_m = \eta_s + \eta_p$ and retardation parameter $\beta = \eta_s/\eta_m$, where η_s and η_p denote the solvent and polymeric viscosity, respectively. The upper and lower boundaries of the domain are set into motion so that sufficiently far away from the drop, the flow is simple shear with shear rate $\dot{\gamma}$. The governing equations for each liquid are incompressibility $\nabla \cdot \mathbf{u} = 0$, and momentum transport

$$\rho \left(\frac{\partial \mathbf{u}}{\partial t} + (\mathbf{u} \cdot \nabla) \mathbf{u} \right) = \nabla \cdot (-p \mathbf{I} + \mathbf{T} + \eta_s [\nabla \mathbf{u} + (\nabla \mathbf{u})^T]) + \mathbf{F}, \quad (1)$$

where \mathbf{T} denotes the extra stress tensor and the surface tension force is computed as a body force \mathbf{F} in the numerical formulation. The Oldroyd-B constitutive model for the matrix liquid is

$$\tau \left(\frac{\partial \mathbf{T}}{\partial t} + (\mathbf{u} \cdot \nabla) \mathbf{T} - (\nabla \mathbf{u}) \mathbf{T} - \mathbf{T} (\nabla \mathbf{u})^T \right) + \mathbf{T} = \eta_p (\nabla \mathbf{u} + (\nabla \mathbf{u})^T), \quad (2)$$

where τ is the relaxation time. Drop deformation in the velocity-velocity gradient plane is defined by $D = (L - B)/(L + B)$, where L and B are the longest and shortest lengths from the center to the interface. The angle of inclination θ is defined to be the angle between the longest axis of the drop and the flow direction. The drop-to-matrix viscosity ratio is denoted $\lambda = \eta_d/\eta_m$. We define the capillary number $Ca = R_0 \dot{\gamma} \eta_m / \Gamma$, where Γ is interfacial tension. A Reynolds number is defined by $Re = \rho \dot{\gamma} R_0^2 / \eta_m$ and is small throughout. A Weissenberg number is $We = \dot{\gamma} \tau$. A dimensionless time is defined by $\hat{t} = t \dot{\gamma}$.

*Electronic address: afkhamis@math.vt.edu; URL: <http://www.math.vt.edu/people/afkhamis>

[†]Electronic address: ptyue@math.vt.edu; URL: <http://www.math.vt.edu/people/ptyue>

[‡]Electronic address: renardy@aol.com; URL: <http://www.math.vt.edu/people/renardy>

II. NUMERICAL RESULTS FOR 2D AND 3D DROP EVOLUTION

Transient 3D simulations are conducted with our in-house volume-of-fluid (VOF) code detailed in Refs. [12–15]. Briefly, the code uses a finite difference methodology on a regular Cartesian mesh. The placement of each fluid is determined by a volume fraction function for one of the liquids in each grid cell. The interface shape is reconstructed with the piecewise linear interface reconstruction scheme, and is advected in a Lagrangian manner by the computed velocity field. Aggarwal and Sarkar [11] developed a numerical methodology based on front-tracking for a 3D transient study of the effect of matrix viscoelasticity on drop deformation in shear flow. Figure 2 shows that our results compare well with the transient and steady state simulations of [11]. It should also be noted that overshoots are not predicted in our simulations, nor in their work.

We focus on $\lambda = 1$, $We = 0.75$, $\beta = 0.5$, at which the 2D numerical study of [16] finds overshoots in deformation; i.e., an initial elongation followed by retraction to stationary state. Ref. [16] uses a diffuse-interface model, in which the interfacial position is determined by a phase-field variable which evolves according to a Cahn-Hilliard formulation. We have independently checked the results of [16] with our volume-of-fluid code and with an initially cylindrical drop in 3D simulations. In particular, we find that the overshoots are not due to inertial effects, because they remain unchanged when the Reynolds number is reduced from 0.1 to 0.02.

We use a computational domain of sides $L_x = 2L_y = 2L_z = 16R_0$ (3D) and $L_x = L_z = 8R_0$ (2D) with x the flow, y the vorticity and z the velocity gradient directions. We found that this domain size is sufficiently large to eliminate boundary effects. We use mesh size $\Delta x = \Delta y = \Delta z = R_0/12$ (3D) and $\Delta x = \Delta z = R_0/12$ (2D) with the timestep of $\Delta t = 0.0001$. We performed a spatial and temporal convergence test at $Re = 0.1, 0.05, 0.02$ and found that results are independent of the mesh size, timestep and Reynolds numbers. For the viscoelastic matrix, we fix the retardation parameter at $\beta = 0.5$, for ease of comparison with the 2D results of [16].

Figure 3 compares the 2D and 3D deformations; in particular, Fig. 3(a) shows the 2D deformation normalized by the stationary state deformation D_S , clearly showing (i) that the overshoot increases as the capillary number is increased; and (ii) for $Ca = 0.5, 0.6$, an undershoot is also observed after the exhibit of the overshoot before the drop reaches a steady shape. Figure 3(b) compares the 2D and 3D deformations, showing the agreement for small $Ca = 0.1, 0.2$. At $Ca = 0.3$, the overshoot in 2D becomes apparent. We therefore examine the viscoelastic stresses at this capillary number. In particular, the extra stress tensor is zero on the Newtonian side, while it grows with time on the viscoelastic side of the interface. Figure 4 shows the trace of the extra stress tensor at $\hat{t} = 1, 2, 3, 4, 12$ for (a) the 2D drop and (b) the 3D.

As shown, viscoelastic stresses grow and then approach to stationary state values by $\hat{t} = 12$. The extra stress tensor is multiplied by the surface area to yield the force exerted on the drop. The initially cylindrical drop has a surface area that extends infinitely in the y direction, while the 3D drop has a concentration of stresses at the tips in a localized round region. Thus, when the 2D and 3D deformations are almost equal, as at $Ca = 0.3$, viscoelastic stresses for the initially cylindrical drop are less than those of the initially spherical drop. This is confirmed in Fig. 4 by examining the temporal evolution of the trace of the extra stress tensor, which is higher in 3D throughout the evolution, pulling out the tip of the drop.

At $\hat{t} = 4$, the 2D drop has already reached maximal deformation and begins retracting, at which time the 3D drop is still elongating. We therefore compare the components of the extra stress tensor at $\hat{t} = 4$. Figure 5 shows contours of the (x,x) , (z,z) and (x,z) components in (a) 2D and (b) 3D simulations. These contribute a surface force equal to $\mathbf{T}\mathbf{n} = (T_{xx}n_x + T_{xz}n_z, T_{xz}n_x + T_{zz}n_z)$ where $\mathbf{n} = (n_x, n_z)$ is the normal at the interface. Normals are indicated with straight arrows in Fig. 5. The dominant component is (x,x) which acts at the tip where the normal to the interface points mostly in the $(-x)$ direction, which contributes to pulling the tip out, with larger magnitude in 3D than in 2D.

The (x,z) component is roughly half of the magnitude of the (x,x) component. The (x,z) component in 2D is positive above the drop where the normal vector, sketched at the interface, points mostly in the z direction. This results in a force that rotates the drop toward the flow direction. The 2D contribution at the drop tip is identified with the normal vector that mostly points in the $(-x)$ direction, with a small contribution in the $(-z)$ direction, resulting in a force that rotates the drop away from the flow direction. Compared to this, the (x,z) extra stress component for the 3D drop has a larger contribution at the drop tip, and rotates it out of the flow direction.

The relatively small (z,z) component in 3D is located along the interface where the normal points mostly in the $(-x)$ direction, perpendicular to the z direction, and therefore contributes little in the way of rotating the drop. The corresponding 2D (z,z) component is placed where the normal to the interface has a nontrivial z -component, which acts to rotate the drop toward the flow direction. Therefore, while the 2D drop rotates and retracts, continued elongation is promoted in 3D.

At $Ca = 0.4$ and higher, the 2D overshoot becomes more pronounced, and the drop settles to stationary state, while the 3D case does not overshoot but breaks above 0.4. To see that extra stresses are always larger in 3D than 2D, we also investigated the $Ca = 0.5$ case at $\hat{t} = 4$ in which the 2D overshoot in deformation is more noticeable. The simulations show qualitatively similar behavior of extra stresses as for the $Ca = 0.3$ case. We noticed an increase in the magnitude of the stress components; however, the placement and the behavior of the

extra stress components are the same as in Fig. 5; we therefore do not show the results of $Ca = 0.5$.

Figure 6 presents the breakup process at $Ca = 0.5$. The drop deforms to form dumbbells which become the first daughter drops, held together by a neck that thins until end-pinching occurs. The contours of the trace of \mathbf{T} show that the stresses build up at the interface outside the tip of the drop, pulling the ends out. The magnitude of maximal stress increases and the placement of the maximal value moves toward the interface, adding to the difficulty in numerical resolution. At $\hat{t} \approx 87.5$, the drop elongates sufficiently to begin end-pinching. In addition to the drop tip area, viscoelastic stress begins to build up at the neck during the necking or pinch-off. After $\hat{t} = 87.5$, the daughter drops move away with the flow, while the filament retracts due to interfacial tension.

We note that the 2D overshoots also occur in the Newtonian-Newtonian system for Stokes flow. For example, it is known that for the case of a Newtonian drop in a Newtonian matrix at $\lambda = 1$, the 2D drop overshoots for sufficiently high capillary numbers such as $Ca = 0.5$. On the other hand, the 3D drop breaks up for $Ca \geq 0.43$ and below this critical capillary number, no overshoots have been found [17–19].

The Newtonian counterpart of Fig. 3 is shown in Fig. 7 also for $\lambda = 1$. Figure 7 shows that as the capillary number increases from 0.1 to 0.6, (i) at $Ca = 0.3$ and higher, the drop deforms more in 3D than in 2D; (ii) a slight overshoot in deformation occurs in 2D but not in 3D; and (iii) 2D droplet deformations reach stationary states at these capillary numbers while the 3D drop breaks up above $Ca = 0.4$. In each case that we have examined, decreased drop deformation correlates with more drop rotation; hence, we next turn our attention to the angle of inclination of the droplet.

Figure 8 shows the steady state angle of inclination θ_s as a function of the final deformation D_s for a Newtonian drop in a viscoelastic matrix ($\lambda = 1, We = 0.75$), and its corresponding Newtonian counterpart ($\lambda = 1$). At the same steady state deformation, the 2D drop (-.-) is more rotated toward the flow direction than the 3D (—). A higher shear rate is required for the cylindrical interface to achieve the same deformation as for the spherical drop (—). To achieve the same amount of deformation, the viscoelastic matrix case is more aligned with the flow direction than the Newtonian-Newtonian system, because the viscoelastic stresses contribute to elongation. For low deformation such as $Ca \sim 0.1$, the 2D simulation predicts the spherical drop evolution well, because the dominant deformation occurs in the velocity-velocity gradient plane, in which both spherical and cylindrical drops project as circular shapes.

III. DEPENDENCE OF OVERSHOOT ON VISCOSITY RATIO

For a Newtonian drop in a Newtonian matrix in Stokes flow, simple shear rotates the drop with an angular velocity of order $\dot{\gamma}$, while the viscous force elongates it at a rate of the order of the viscous stress on the drop divided by η_d . The viscous stress arises from the product of the matrix viscosity with shear rate. The mechanism for settling to a steady shape is drop rotation towards the flow direction, away from the extensional axis that is at 45 degrees to the flow direction. Thus, the drop cannot break if the rotation rate is much larger than the deformation rate: $\dot{\gamma} \gg (\eta_m \dot{\gamma})/\eta_d$ or $\lambda \gg 1$ [20]. Experimentally and theoretically, it is known that there is a critical viscosity ratio of roughly 3.1 beyond which the drop does not break. We shall show that the 3D viscoelastic matrix case also rotates and retracts to a stationary state at higher viscosity ratios, reminiscent of the qualitative features of the 2D overshoot discussed in the prior section.

Figure 9(a) shows transient drop deformations for the experimental data of [5] at $Ca = 0.43, We = 0.645$, while varying the viscosity ratio λ from 2 to 8. This figure shows that the overshoots increase with increasing λ . For $\lambda = 8$, the capillary number is increased to $Ca = 0.6$ (- -), which yields a higher overshoot since viscous shear initially elongates the drop more than at $Ca = 0.43$. Figure 9(b), shows the evolution of the drop inclination angle. On increasing λ , we observe decrease in θ , and decrease in the steady state deformation. Similarly, a significant overshoot is also observed in the transient deformation of a Newtonian drop-Newtonian matrix system at a sufficiently large viscosity ratio. In Fig. 9(a) and (b), the transient drop deformation and inclination angle are shown also for a Newtonian drop in a Newtonian matrix at $Ca = 0.43$ and $\lambda = 8$ (-.-). This demonstrates that for $\lambda = 8$, even a Newtonian drop-Newtonian matrix system shows overshoot under shear. Small deformation theory [21] and experiments [22] confirm the oscillations in deformation in a Newtonian system when λ is large.

A comparison of Figs. 9(a) and (b) shows that the retraction in D corresponds to the angle of orientation aligning more with the flow direction. The case $\lambda = 8, Ca = 0.6$ (- -), shows a marked overshoot and undershoot in deformation and angle before reaching a steady shape. Viscoelastic stresses that develop in response to shear elongate the drop further, but only after a time scale determined by the relaxation time. Depending on the balance of viscous and viscoelastic effects, if the drop has not reached a critical length before aligning with the flow direction, it retracts instead of breaking. This overshoot becomes more pronounced with increasing viscosity ratio with other parameters fixed. At higher viscosity ratios, overshoots and undershoots are amplified with increasing capillary number.

Drop deformation in 3D at $\lambda = 1$ for a viscoelastic matrix at $We = 0.75, \beta = 0.5$, is qualitatively different from 2D in that the 2D drop elongates and then retracts while the 3D drop evolves gradually toward a steady state and to breakup for sufficiently large Ca . A comparison of the extra stress tensor for 2D and 3D shows that there is a viscoelastic wake located at a short distance away from the drop tip, extending outward, where the dominant viscoelastic stress is the (x,x) component which pulls the tip out. The (x,z) and (z,z) components in 2D add more rotation toward the flow direction, while the 3D case remains at a higher angle of inclination. Once a drop rotates to

the flow direction, it lies in a region of low velocities; both viscous force and viscoelastic force decrease and the drop retracts. Rotation is promoted when the viscosity ratio increases past 1, and this contributes to overshoots in transient deformation history.

Acknowledgments

This research is supported by NSF-DMS-0456086, NCSA TG-CTS060013N. We thank Andres Avila for the use of the CEMCC, Universidad de La Frontera SGI Altix system.

-
- [1] K. Verhulst, R. Cardinaels, P. Moldenaers, Y. Renardy, and S. Afkhami. Influence of viscoelasticity on drop deformation and orientation in shear flow. Part 1: Stationary states. *J. Non-Newtonian Fluid Mech.*, 156:29–43, 2009.
- [2] S. Guido, M. Simeone, and F. Greco. Deformation of a Newtonian drop in a viscoelastic matrix under steady shear flow. Experimental validation of slow flow theory. *J. Non-Newtonian Fluid Mech.*, 114:65–82, 2003.
- [3] S. Guido, M. Simeone, and F. Greco. Effects of matrix viscoelasticity on drop deformation in dilute polymer blends under slow shear flow. *Polymer*, 44:467–471, 2003.
- [4] S. Guido and F. Greco. Dynamics of a liquid drop in a flowing immiscible liquid. In D. M. Binding and K. Walters, editors, *Rheology Reviews*, pages 99–142. British Society of Rheology, Aberystwyth, Wales, 2004.
- [5] V. Sibillo, M. Simeone, and S. Guido. Break-up of a Newtonian drop in a viscoelastic matrix under simple shear flow. *Rheol. Acta*, 43:449–456, 2004.
- [6] V. Sibillo, S. Guido, F. Greco, and P.L. Maffettone. Single drop dynamics under shearing flow in systems with a viscoelastic phase. In *Times of Polymers, Macromolecular Symposium 228*, pages 31–39. Wiley-VCH Berlin, 2005.
- [7] K. Verhulst, P. Moldenaers, and M. Minale. Drop shape dynamics of a Newtonian drop in a non-Newtonian matrix during transient and steady shear flow. *J. Rheol.*, 51:261–273, 2007.
- [8] K. Verhulst, R. Cardinaels, P. Moldenaers, S. Afkhami, and Y. Renardy. Influence of viscoelasticity on drop deformation and orientation in shear flow. Part 2: Dynamics. *J. Non-Newtonian Fluid Mech.*, 156:44–57, 2009.
- [9] V. Cristini, R. W. Hooper, C. W. Macosko, M. Simeone, and S. Guido. A numerical and experimental investigation of lamellar blend morphologies. *Ind. Eng. Chem. Res.*, 41:6305–6311, 2002.
- [10] N. Aggarwal and K. Sarkar. Deformation and breakup of a viscoelastic drop in a Newtonian matrix under steady shear. *J. Fluid Mech.*, 584:1–21, 2007.
- [11] N. Aggarwal and K. Sarkar. Effects of matrix viscoelasticity on viscous and viscoelastic drop deformation in a shear flow. *J. Fluid Mech.*, 601:63–84, 2008.
- [12] J. Li, Y. Renardy, and M. Renardy. Numerical simulation of breakup of a viscous drop in simple shear flow through a volume-of-fluid method. *Phys. Fluids*, 12:269–282, 2000.
- [13] Y. Renardy, M. Renardy, T. Chinyoka, and D. B. Khismatullin. A viscoelastic VOF-PROST code for the study of drop deformation. *Proc. ASME Heat Transfer/Fluids Engineering Summer Conference*, pages HT-FED2004-56114, ASME Press New York, 2004.
- [14] T. Chinyoka, Y. Renardy, M. Renardy, and D. B. Khismatullin. Two-dimensional study of drop deformation under simple shear for Oldroyd-B liquids. *J. Non-Newtonian Fluid Mech.*, 130:45–56, 2005.
- [15] D. Khismatullin, Y. Renardy, and M. Renardy. Development and implementation of VOF-PROST for 3d viscoelastic liquid-liquid simulations. *J. Non-Newtonian Fluid Mech.*, 140:120–131, 2006.
- [16] P. Yue, J. J. Feng, C. Liu, and J. Shen. Transient drop deformation upon startup of shear in viscoelastic fluids. *Phys. Fluids*, 17:123101–123107, 2005.
- [17] Y. Renardy and M. Renardy. PROST: a parabolic reconstruction of surface tension for the volume-of-fluid method. *J. Comput. Phys.*, 183(2):400–421, 2002.
- [18] R. Hooper, V. Cristini, S. Shakya, J. S. Lowengrub, C. W. Macosko, and J. J. Derby. Modeling multiphase flows using a novel 3d adaptive remeshing algorithm. In *Computational Methods in Multiphase Flow, Advances in Fluid Mechanics*, volume 29, pages 33–42. Wessex Institute of Technology Press, Southampton, UK, 2001.
- [19] X. Zheng, J. Lowengrub, A. Anderson, and V. Cristini. Adaptive unstructured mesh -II. Application to two- and three-dimensional level-set simulations of multiphase flow. *J. Comput. Phys.*, 208:626–650, 2005.
- [20] D. Khismatullin, Y. Renardy, and V. Cristini. Inertia-induced breakup of highly viscous drops subjected to simple shear. *Phys. Fluids*, 15 (5):1351–1354, 2003.
- [21] J. M. Rallison. Note on the time-dependent deformation of a viscous drop which is almost spherical. *J. Fluid Mech.*, 98(3):625–633, 1980.
- [22] S. Torza, R. G. Cox, and S. G. Mason. Particle motions in sheared suspensions: transient and steady deformation and burst of liquid drops. *J. Colloid Interface Sci.*, 38:395–411, 1972.

1. Deformation (top) and angle of inclination (bottom) as a function of dimensionless time for a Newtonian drop in a viscoelastic matrix at $\lambda = 1.5$, $Ca = 0.36$, and $We = 2.12$. Experimental data from [1] (\circ), Oldroyd-B model simulation 3D (—) and 2D (- -).
2. Newtonian drop deformation in viscoelastic matrix. Numerical simulations at $We = 1$ (—) and $We = 2$ (- -) are compared with the numerical simulations of [11], $We = 1$ (\circ) and $We = 2$ (\triangleright), at $\lambda = 1$, $\beta = 0.5$, $Ca = 0.3$, $Re = 0.1$.
3. Evolution of deformation for a Newtonian drop in a viscoelastic matrix at $\lambda = 1$, $We = 0.75$, $Ca = 0.1$ (\circ), 0.2 (\square), 0.3 (∇), 0.4 (\diamond), 0.5 (\triangle), 0.6 (\triangleright). (a) 2D numerical simulations normalized by the stationary state showing relative magnitude of overshoots which increase with capillary number; (b) 2D (—) and 3D (- -) simulations for total deformation D .
4. Newtonian drop in viscoelastic matrix. Contours of the trace of the extra stress tensor at $\lambda = 1$, $Ca = 0.3$, and $We = 0.75$, in the x-z cross-section of the drop. $\hat{t} = 1, 2, 3, 4, 12$. (a) 2D (— in Fig. 3) (b) 3D (- - in Fig. 3).
5. Contours of extra stress tensors are compared for the (x,x), (x,z) and (z,z) components of (a) 2D, and (b) 3D simulations, $\lambda = 1$, $Ca = 0.3$, $We = 0.75$, $\hat{t} = 4$. Normals at the interface are indicated by straight arrows.
6. Drop shapes and contours of the trace of the extra stress tensor are shown for 3D breakup of a Newtonian droplet in a viscoelastic matrix, in the x-z cross-section of the drop, $\lambda = 1$, $Ca = 0.5$, $We = 0.75$. $\hat{t} = 50, 87.5, 96.25$.
7. Evolution of deformation for a Newtonian drop in a Newtonian matrix at $\lambda = 1$. $Ca = 0.1$ (\circ), 0.2 (\square), 0.3 (∇), 0.4 (\diamond), 0.5 (\triangle), 0.6 (\triangleleft); 2D (—) and 3D (- -) simulations.
8. Stationary state orientation angle θ_s vs. the stationary state deformation D_s . Newtonian drop in a Newtonian matrix (\circ) for $\lambda = 1$ and Newtonian drop in a viscoelastic matrix (\triangle) for $\lambda = 1$ and $We = 0.75$. 2D (- -) and 3D (—) results are compared.
9. (a) 3D drop deformation D and (b) drop inclination angle θ vs. dimensionless time, for $\lambda = 2$ (\square), 4 (∇), 8 (\triangle) at fixed $Ca = 0.43$, $We = 0.645$, and the case $\lambda = 8$, $Ca = 0.6$ (\triangleleft). In (b), the latter case has a negative angle or an undershoot in θ between $\hat{t} \approx 6.5$ and 10. Newtonian drop in a Newtonian matrix at $Ca = 0.43$ and $\lambda = 8$ (- -) is also plotted.

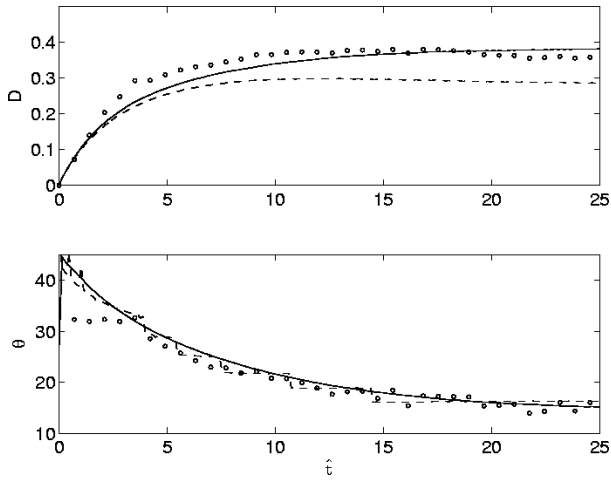


FIG. 1: Deformation (top) and angle of inclination (bottom) as a function of dimensionless time for a Newtonian drop in a viscoelastic matrix at $\lambda = 1.5$, $Ca = 0.36$, and $We = 2.12$. Experimental data from [1] (\circ), Oldroyd-B model simulation 3D (—) and 2D (- -).

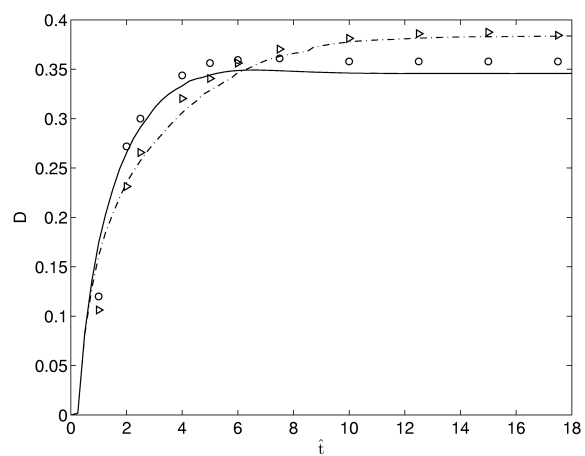


FIG. 2: Newtonian drop deformation in viscoelastic matrix. Numerical simulations at $We = 1$ (—) and $We = 2$ (- -) are compared with the numerical simulations of [11], $We = 1$ (\circ) and $We = 2$ (\triangleright), at $\lambda = 1$, $\beta = 0.5$, $Ca = 0.3$, $Re = 0.1$.

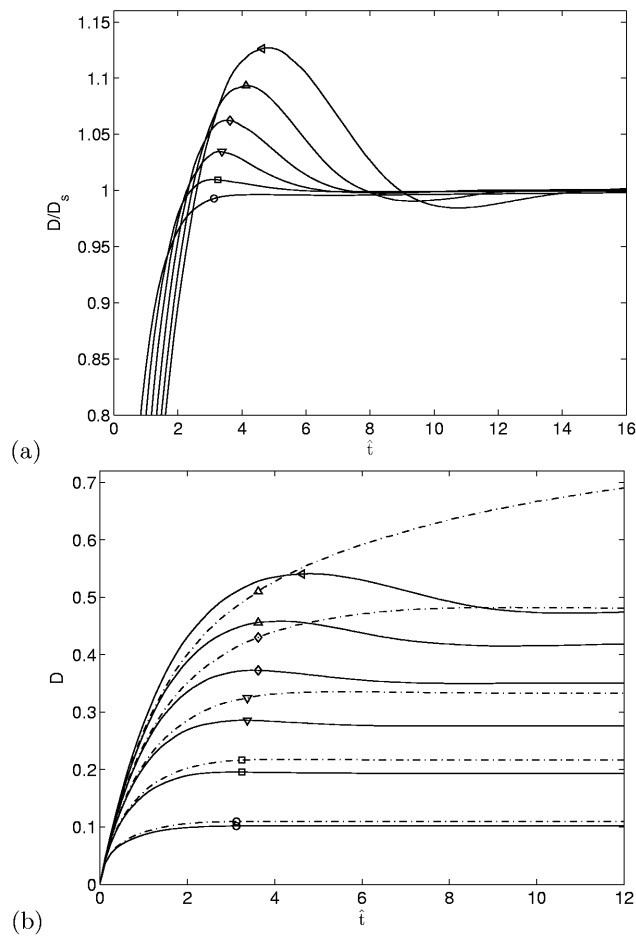


FIG. 3: Evolution of deformation for a Newtonian drop in a viscoelastic matrix at $\lambda = 1$, $We = 0.75$, $Ca=0.1$ (\circ), 0.2 (\square), 0.3 (∇), 0.4 (\diamond), 0.5 (\triangle), 0.6 (\triangleright). (a) 2D numerical simulations normalized by the stationary state showing relative magnitude of overshoots which increase with capillary number; (b) 2D (—) and 3D (---) simulations for total deformation D .

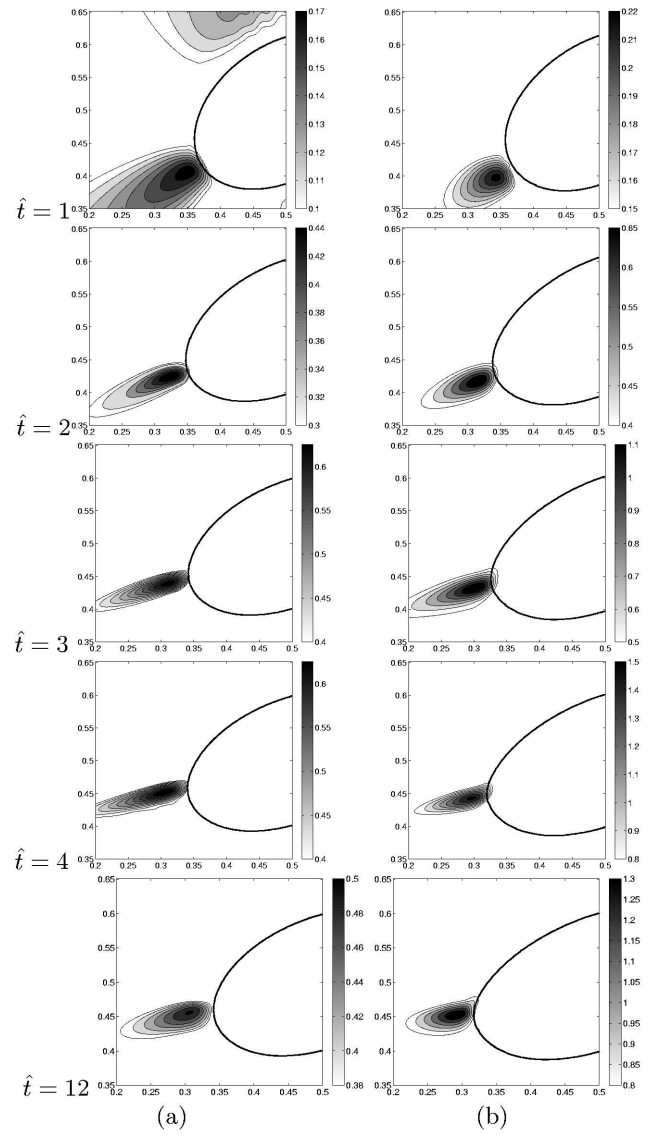


FIG. 4: Newtonian drop in viscoelastic matrix. Contours of the trace of the extra stress tensor at $\lambda = 1$, $Ca = 0.3$, and $We = 0.75$, in the x - z cross-section of the drop. $\hat{t} = 1, 2, 3, 4, 12$. (a) 2D (— in Fig. 3) (b) 3D (--- in Fig. 3).

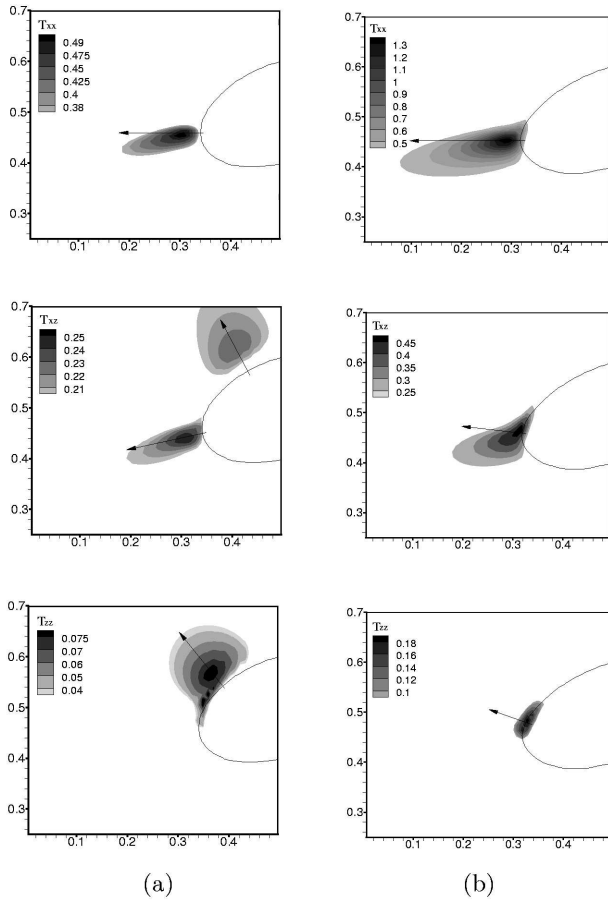


FIG. 5: Contours of extra stress tensors are compared for the (x,x), (x,z) and (z,z) components of (a) 2D, and (b) 3D simulations, $\lambda = 1$, $Ca = 0.3$, $We = 0.75$, $\hat{t} = 4$. Normals at the interface are indicated by straight arrows.

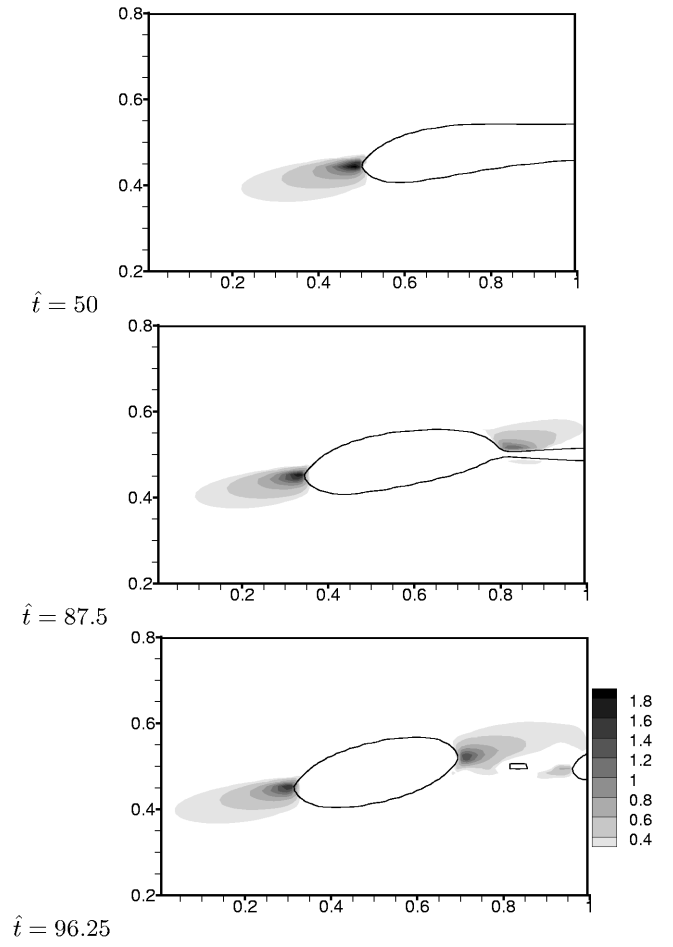


FIG. 6: Drop shapes and contours of the trace of the extra stress tensor are shown for 3D breakup of a Newtonian droplet in a viscoelastic matrix, in the x-z cross-section of the drop, $\lambda = 1$, $Ca = 0.5$, $We = 0.75$. $\hat{t} = 50, 87.5, 96.25$.

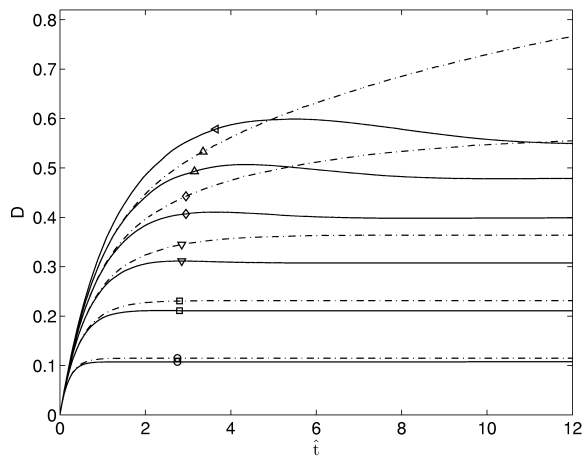


FIG. 7: Evolution of deformation for a Newtonian drop in a Newtonian matrix at $\lambda = 1$. $Ca=0.1$ (\circ), 0.2 (\square), 0.3 (∇), 0.4 (\diamond), 0.5 (\triangle), 0.6 (\triangleleft); 2D (—) and 3D (-.-) simulations.

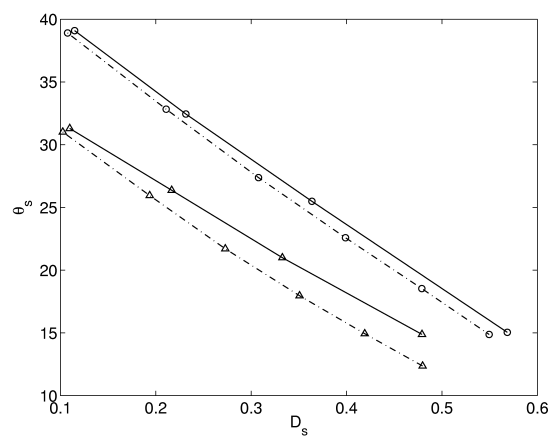


FIG. 8: Stationary state orientation angle θ_s vs. the stationary state deformation D_s . Newtonian drop in a Newtonian matrix (\circ) for $\lambda = 1$ and Newtonian drop in a viscoelastic matrix (\triangle) for $\lambda = 1$ and $We = 0.75$. 2D (-.-) and 3D (—) results are compared.

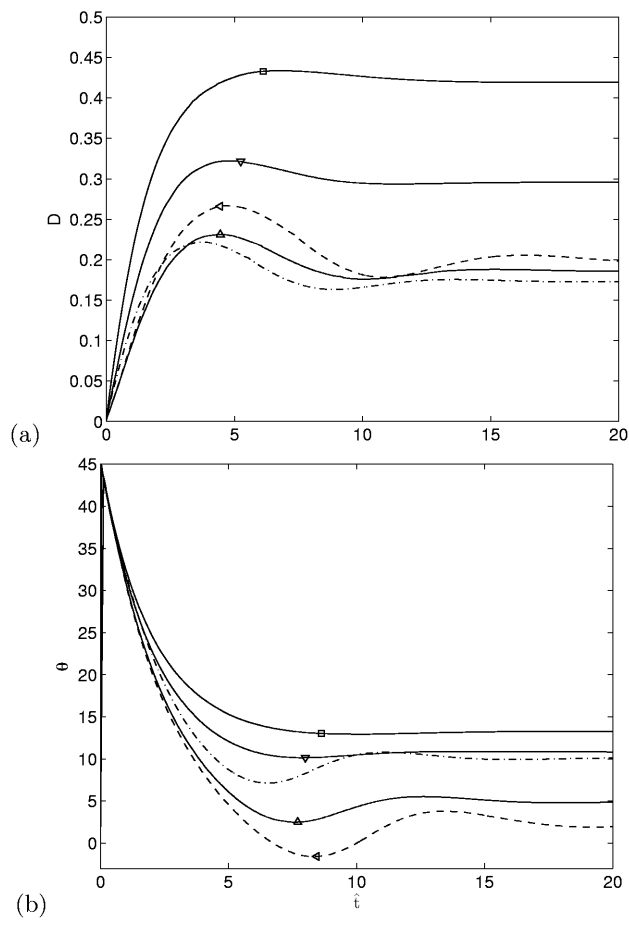


FIG. 9: (a) 3D drop deformation D and (b) drop inclination angle θ vs. dimensionless time, for $\lambda=2$ (\square), 4 (∇), 8 (\triangle) at fixed $Ca = 0.43$, $We = 0.645$, and the case $\lambda=8$, $Ca = 0.6$ (\triangleleft). In (b), the latter case has a negative angle or an undershoot in θ between $\hat{t} \approx 6.5$ and 10. Newtonian drop in a Newtonian matrix at $Ca = 0.43$ and $\lambda = 8$ (-.-) is also plotted.